Terra MODIS sees solar eclipses: Analysis of reflective solar band response at multiple radiance levels

Gal Sarid[a], Kevin A. Twedt[a], and Xiaoxiong Xiong[b]

[a]Science Systems and Applications Inc., Lanham, MD 20706, USA
[b]Sciences and Exploration Directorate, NASA/GSFC, Greenbelt, MD 20771, USA

ABSTRACT

The MODIS imaging spectroradiometer instruments on-board NASA's Terra and Aqua satellites have 20 reflective solar bands (RSB) covering a wavelength range from 400 to 2200 nm. Radiance is calculated from processing raw signals with background, temperature, and electronic contamination corrected. Measured gain is calibrated with a fully Sunlit solar diffuser (SD) at a stable radiance level, considering a slowly changing SD reflectance degradation. These measurements provide time-dependent gain adjustment factors, and the calibration assumes a linear response for each band and detector. Hence, an analysis of the dependence on different radiance levels is warranted. The MODIS design has no mechanism for varying radiance levels, except for an attenuator screen. However, it has been in static configuration for Terra since mid-2003. An external source of radiance attenuation can be utilized during solar eclipse events, while maintaining high stability and accuracy of solar calibration standards. Due to its long mission lifetime, Terra has seen several Sun-Moon near-conjunction events when it coincides with the orbit path where the SD is directly illuminated. As of August 2020, we have identified 7 viable partial solar eclipses in the Terra mission data. We will discuss several results of our study, including comparison of measured SD signal to predicted radiance reduction based on a solar disk radiance model; nominal and outlier behavior as a function of bands, detectors, and mirror-sides; and comparison with other data sets. Our main conclusion from this study is that there is no notable correlation of detector-dependent trend with radiance level for most RSB bands.

Keywords: Terra, MODIS, Reflective Solar Bands, Solar Eclipse

1. INTRODUCTION

The Moderate Resolution Imaging Spectroradiometer (MODIS) instrument is one of the key components of NASA's Earth Observing System (EOS). It was launched aboard the Terra and Aqua spacecrafts in December 1999 and May 2002, respectively, and began routine operations shortly thereafter. MODIS provides daily global imagery for the study of the Earth's land, ocean, and atmosphere, with satellite orbits enabling the entire Earth's surface to be viewed every two days. MODIS has a total of 36 spectral bands covering the range of 400-14400 nm, of which we focus here on the 20 reflective solar bands (RSB). These bands cover a wavelength range of 400-2200 nm, which are in the visible to visible to short-wave infra-red (IR) range, and are set up at varying spatial resolutions – 250 m for bands 1 and 2 (40 detectors per band), 500 m for bands 3-7 (20 detectors per band), and 1 km for bands 8-19 and 26 (10 detectors per band). The radiance of each MODIS RSB detector is calculated from dn^*, which is the digital count number dn corrected for temperature effects (crosstalk contamination correction is applied to some bands or detectors, but not in this study). The latter is the processed raw signal in digital counts (DN) with background subtraction. dn^* is used as the base signal for all data analyses and calibrations. On-orbit radiometric calibration is analyzed to track RSB gain changes by using observations of a Sunlit solar diffuser (SD), which views the Sun through an optional attenuation screen.[1] The SD observations are made at a similar radiance level every orbit and provide time-dependent calibration factors (m_1) to adjust the measured gain of each band and detector.[1] The on-orbit degradation of the SD due to solar radiation is tracked using the SD Stability Monitor (SDSM) with 9 designated detectors. In its original configuration, the SD door (SDD) shields the SD surface from solar exposure and can be moved from closed to open state for SD calibration events.

Send correspondence to:
G.S.: E-mail: gal.sarid@ssaihq.com, Telephone: +1-301-867-6342

In addition, an SD screen (SDS) is in place to shield high-gain RSB detectors from direct Sunlight saturation during calibration events. While this is still the case for Aqua MODIS, Terra MODIS experienced an SDD anomaly in mid-2003, leaving it in a constant configuration of SDD open and SDS closed.[1] As a result of these configurations for the Terra MODIS RSB, there is no on-orbit mechanism for calibration at multiple radiance levels. Hence, there is no independent test to examine the working assumption of gain linearity for different bands and detectors.

Due to their long mission lifetimes, the Terra and Aqua satellites have had a chance to pass through Sun-Moon near-conjunction events, which may correspond to varying levels of partial solar eclipses observed with the MODIS instrument as the SD is directly illuminated by the Sun. As of August 2020, we are able to identify and pick out 7 partial solar eclipse events in the Terra historical mission data. For Aqua, the SDD has always been closed during past eclipse events, so no data are available. For future dates, we can plan to schedule SD calibrations during these events so that SDD open data can be collected.

Solar eclipse events represent stable radiance attenuation circumstances, which do not depend on uncertainties or degradation of on-board attenuation mechanisms. It is a celestial occurrence that maintains the high stability and accuracy of the solar calibration standard with a reduction in radiance that can be wavelength-dependent. Except for the S-NPP and NOAA-20 VIIRS study,[2] which our current work continues, eclipse events have gone largely unobserved or unstudied in the field of remote sensing calibration. One exception is the Operational Land Imager on Landsat-8, which performed observations of a solar eclipse event in 2014,[3,4] but a detailed study of the solar calibration during this event has not been presented.

In this paper, we analyze the solar eclipse events observed by the MODIS SDs and use them to compare SD signal to predicted radiance reduction, examine nominal and outlier behavior of band and detector responses, and evaluate the on-orbit validation of gain linearity. We use the Sun and Moon geometry and a model of the solar radiance to predict the expected reduction in radiance and compare it to the reduction measured per band per detector by MODIS. Our approach starts with identification of partial eclipse events in the all-mission data set with a simple geometric model and selection of robust events for further analysis. We then calculate the modeled solar radiance, as should be seen by the MODIS SD, and the expected reduction in radiance corresponding to the wavelength range of the RSB and elevation angles for the SD viewing geometry. Lastly, we compute the measured reduction in radiance from the ratio of the gain responses (dn values) that are recorded for the eclipsed and the non-eclipsed orbits of the same day. We find that radiance level dependent features can be characterized for each band and detector, with examples of this analysis as a diagnostic application for both identified and unknown minor trends. In addition, we find that the discrepancy between modeled and measured radiance reduction per band and per detector increases with increasing eclipse depth, and that there is a varying scatter in the signal responses, with the high-gain bands (bands 8-16) having the smallest variance. At the conclusion of this paper, we also briefly discuss the uncertainties and limitations of this approach and its applicability to other remote sensing instruments.

2. SOLAR ECLIPSE CIRCUMSTANCES

Solar eclipse events can be identified by the solar vector and lunar vector information stored in the MODIS on-board calibration (OBC) data files. The SD calibration occurs when the SD view port is directly illuminated by the Sun, corresponding to when Terra crosses the high latitude Northern hemisphere on the night side of the Earth. For the MODIS SD to be able to view the partial or total eclipse, the eclipsed region of space must extend through low-Earth orbit over the North Pole. For initial estimates of whether eclipse events will be recorded by the Terra MODIS instrument, we use a simple model to calculate the Sunlight fraction transmitted past the Moon. This consists of a simplified geometric setup that includes the area overlap between two circles, which have the projected sizes of the Sun and Moon respectively, distances from the satellite at that point in time in the orbit, and the solar and lunar vectors, as recorded in the L1B OBC data files for that point in time in the orbit. A schematic representation of the eclipse geometry between the satellite orbit and the eclipse region in space is shown in Fig. 1. As mentioned previously, the companion Aqua satellite does not have SD calibration data available during past eclipse events.

In order for an orbit to be classified as a robust partial eclipse event for our analysis, the following conditions should be satisfied:

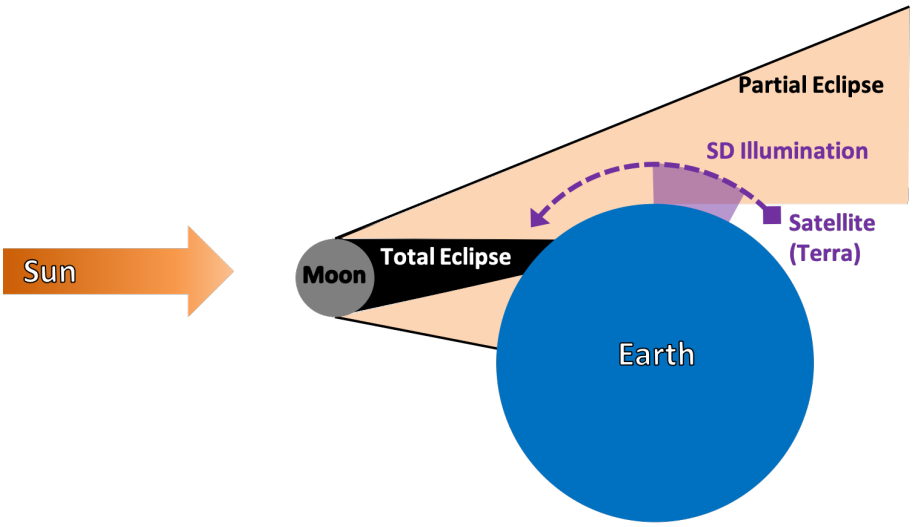

Figure 1: Schematic of the geometry of a solar eclipse event as viewed by Terra MODIS during SD calibrations. The orange shaded region represents the partial eclipse projected region in space, which crosses the satellite's orbit. The purple shaded region represents the section of the satellite orbit when the SD is illuminated by the Sun.

- Sun-Moon angle < 0.56 degrees, which is the maximum of the Moon/Sun angular radius.
- Extended solar elevation angle range that optimizes the SD signal responses for calibration events, which is the SD "sweet-spot" range of $8 - 16$ degrees.[1]
- SD pointing towards the Sun, where the spacecraft-Sun vector has x-axis component > 0.

Table 1 lists the analyzed solar eclipse events as viewed by Terra MODIS over the mission lifetime through August 2020. The solar radiance reduction due to the different partial eclipse circumstances covers the range recorded by the responses of the different bands and detectors. This happens during the time that the satellite crosses through the projected path and the MODIS SD is aligned to observe the partial eclipse.

Table 1: Listing of solar eclipse events viewed by Terra MODIS. The reduction in solar radiance is the drop in the observed signal on the SD during the eclipse orbit in the sweet-spot of the SD calibration. The range represents the variation with time and with wavelength.

Event Date	**Orbit ordinal**	**Solar Radiance Reduction**
March 19, 2007	3	10% – 12%
June 1, 2011	14	30% – 32%
May 21, 2012	1	3% – 5%
October 23, 2014	13	33% – 37%
March 20, 2015	7	83% – 89%
August 11, 2018	6	65% – 69%
January 6, 2019	1	26% – 29%

The most significant eclipse event happened on March 20, 2015, with over 80% reduction in radiance. In general, the partial eclipse events that were observed with MODIS cover a range of radiance reduction of $0.03 -$

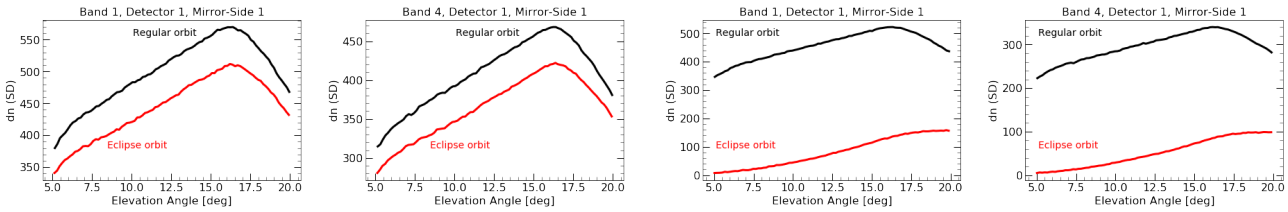

(a) March 19, 2007 (b) March 20, 2015

Figure 2: Measured MODIS SD signal as a function of the solar elevation angle, during an eclipse orbit compared to a neighboring non-eclipsed orbit for two distinct events. Bands 1 and 4 are shown for mirror-side 1 and detector 1 as examples of different spatial resolutions.

0.89, when considering all the RSB bands and detectors. The middle column of Table 1 lists the ordinal number of the eclipsed orbit for that event day. An eclipse event can be recorded as a raw signal reduction during two consecutive orbits. That happened on January 6, 2019, so for that case, we considered only the orbit with the largest eclipse magnitude and did not include the other eclipsed orbit in the analysis.

Fig. 2 shows two examples comparing the SD signal measured by MODIS for bands 1 and 4 (detector 1 and mirror-side 1), which represent different spatial resolutions of the MODIS RSB. The eclipsed orbit and an adjacent non-eclipsed orbit are plotted in red and black, respectively, as the dn signal across the elevation angle. The y-axis corresponds to the sensor's response after the space view (SV) background subtraction ($DN_{SD} - DN_{SV}$) and temperature correction, which depends on the instrument temperature at the Earth view (EV) observation time and temperature reference values determined pre-launch.[1] The reduction in signal is clearly seen across the SD extended sweet-spot elevation angle range ($8 - 16$ degrees), as well as outside of it. We note that for the deeper event (March 20, 2015, Fig. 2b), there is a change in the trend of dn across the elevation angle between the eclipsed and non-eclipsed orbits. This is due to the motion of the Terra satellite during the duration of the partial eclipse event (see also Fig. 1). Since the solar radiance is strongly reduced, the effective result of the SD being illuminated at a higher elevation angle means that the fraction of the eclipsed region in space that the SD observes is smaller. This causes the measured signal to be higher compared with smaller elevation angles during the same event.

3. DATA SELECTION AND ANALYSIS

After identifying the partial solar eclipse events in the all-mission data set (Sec. 2), we need to calculate the measured Sun fraction from the SD signals. We then compare it to the modeled Sun fraction, as seen by the MODIS SD for a derived wavelength range covering the RSB bands and elevation angle range covering the SD illumination section of $5 - 20$ degrees.

We first look at the MODIS RSB SD calibration procedure. In general, the EV radiance is defined as

$$L_{EV} = \frac{\rho_{EV} \cdot \cos(\theta_{EV}) \cdot E_{Sun}}{d_{ES}^2}, \tag{1}$$

where ρ_{EV} is the EV scene reflectance, θ_{EV} is the solar zenith angle, d_{ES} is the Earth-Sun distance (in AU, at EV scene observation time), and E_{Sun} is the solar irradiance (at 1 AU distance, normalized by π). The reflectance factor is defined as

$$\rho_{EV} \cdot \cos(\theta_{EV}) = \frac{m_1 \cdot dn^*_{EV} \cdot d_{ES}^2}{RVS}, \tag{2}$$

where RVS is the response at the scan angle of the EV pixel, dn^*_{EV} is the corrected signal in the EV scene, and $m1$ is the RSB calibration coefficient. The latter is determined from on-orbit SD measurements per band, detector, sub-frame and mirror-side. It is calculated as

$$m_1 = \frac{\rho_{SD} \cdot \cos(\theta_{SD})}{dn^*_{SD} \cdot d_{ES}^2} \cdot \Delta_{SD} \cdot \Gamma_{SD}, \tag{3}$$

where ρ_{SD} is the SD bi-directional reflectance factor (BRF, determined pre-launch), θ_{SD} is the solar zenith angle at the SD scan time, dn^*_{SD} is the corrected signal during SD observation (similarly to the aforementioned dn^*), and Δ_{SD} and Γ_{SD} are the SD plate degradation factor and SD screen vignetting function, respectively.

Combining the above expressions, we can represent the radiance during SD observations as L_{SD} and rearrange all the terms with an 'SD' notation. Assuming that the solar radiance reduction does not vary significantly with wavelength and that the RSB calibration factor m_1 is the same between eclipsed and non-eclipsed orbits for the same day, we can represent the reduction factor between these orbits as

$$A_{eclipse} = \frac{L_{SD,eclipse}}{L_{SD}} = \left(\frac{dn^*_{eclipse}}{dn^*}\right)_{SD}. \tag{4}$$

In this expression, we assumed that during an eclipse event, solar radiance is reduced, but the SD observation is otherwise the same. All other terms, except for the SD signal, are similar. While on longer timescales, the SD degradation and vignetting function can have non-negligible differences, when we compare SD measurements within the same day, these can be considered stable and will cancel out in computing the radiance ratio.

We calculate the measured $A_{eclipse}$ for each scan during the eclipse orbit. This is a time-dependent function of the solar angles and the detector response dn, which we convert to an elevation angle dependency for each band, detector and mirror-side during each of the eclipse events. In practice, we calculate this measured Sun fraction from the ratio of the SD gain ratio of eclipsed orbit to the average of all non-eclipsed orbits during the corresponding day. The SD gain response is calculated per band, detector, sub-frame, and mirror-side. We fit all orbits to the center of the SD sweet-spot range (12.5 degrees) so that we can take into account the small viewing or illumination discrepancies between different orbits. Fig. 3 shows an example of the Sun fraction as a function of elevation angle for the eclipse orbit of August 11, 2018. The different panels show the specific response of detectors $6-15$ for band 3 and mirror-side 1. The measured Sun fraction, which is shown in black in Fig. 3, is calculated at the center of the sweet-spot range with a quadratic fit over a small range of the elevation angles. The modeled Sun fraction, which is shown in red in Fig. 3, is derived for the same band wavelength and interpolated across the same elevation angle range as the measured values (for model details, see discussion for Eq. 5 and 6). In this example, the differences between the measured and modeled Sun fraction for each individual band, mirror-side, and detector are below 2%. For different band, mirror-side and detector combinations, the maximum difference is on the order of a few percent (see Sec. 4.1 for more discussion of the results).

In order for us to be able to evaluate the performance of the SD measurements during eclipse events, we need to compare the measured solar radiance reduction with an independent model of the solar radiance at wavelengths corresponding to the RSB. This model should provide the solar radiance reduction factor ($A_{eclipse}$) during an eclipse event, which is based on solar and lunar geometry. In addition, the model should include the solar limb darkening effect, which has a wavelength dependent radial profile of the radiance from the solar disk. We construct an empirical solar disk radiance model, which includes empirical fitting of multiple solar radiance data sets in the visible to IR wavelength[2,5] so that the derived range covers the MODIS RSB wavelengths.

For this model to be accurate, the relative positions of the Sun and Moon are required at high precision in the Terra coordinate system for the time series of the SD measurement signals. The time stamps stored in the NASA L1B OBC files for each scan correspond to the middle of the SD sector observation. We note that the values of the Sun and Moon vectors stored in the full OBC data files do not have sufficient accuracy for our analysis, which is highly sensitive to the exact angle between the Sun and Moon. For that reason, we use the time stamp information from the OBC files for each event to gather relevant geometry information from the SPICE toolkit. SPICE is NASA's system for observation geometry parameters relevant for various space science missions, which is maintained by the Navigation and Ancillary Information Facility (NAIF), and contains a large collection of data sets and utility programs that supports calculation of positions, vlocities, orientations, reference frames, etc.[6,7]

We use the SPICE toolkit to extract the Sun and Moon positions and the spacecraft attitude at each scan time during an eclipsed orbit. We then calculate the modeled Sun fraction within the range of elevation angles relevant for the SD sweet-spot by interpolating over an extended range of $5-20$ degrees and comparing to the sweet-spot center. Fig. 3 shows an example of this for the August 11, 2018 event, with examples of detectors

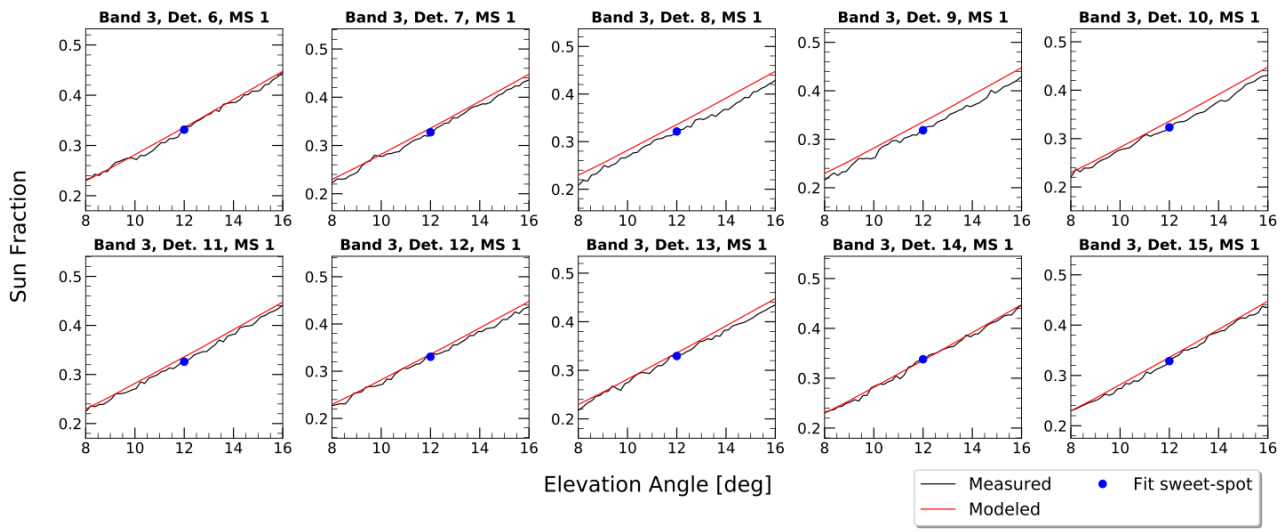

Figure 3: Sun fraction vs. elevation angle for the August 11, 2018 event. Shown are a few examples of individual detector responses (detectors $6-15$) for band 3 and mirror-side 1. Black lines are the measured responses and red lines are the modeled reduction values. Note that measured values have been fitted to the center of the SD sweet-spot at 12.5 degrees (blue dot).

$6-15$ for band 3 and mirror-side 1. All values are increasing with elevation angle, since the SD is able to see a larger fraction of the solar radiance, either in the eclipsed or non-eclipsed orbits (see illustration in Fig. 1. Note that all modeled values are the same between the different panels of Fig. 3 because the model only depends on wavelength (i.e. MODIS band), so there is no detector-dependent information.

We model the solar limb darkening by considering the solar disk intensity relative to the intensity at the center of the disk, following Twedt et al. 2019.[2] In the MODIS RSB wavelength range, the following expression represents the distribution accurately:

$$\Gamma(r,\lambda) = \frac{I(r,\lambda)}{I(r=0,\lambda)} = \left(1 - \frac{r^2}{R_S^2}\right)^{\alpha(\lambda)/2} \quad ; \quad \alpha = -0.023 + (292\mu m)/\lambda. \tag{5}$$

In this expression, r is the radial position from the disk center, R_S is the radius of the Sun, and α is a wavelength-dependent exponent controlling the limb darkening relative strength across the solar disk. The intensity I is largest at the disk center and drops off toward the edge. There is a steeper drop for shorter wavelengths, based on data from solar observations. To determine the total wavelength-dependent intensity of the solar disk when it is partially obscured by the Moon, we must integrate the above expression over the section of the Sun that is not obscured by the Moon, as observed at the location of Terra during an eclipse event. The geometry for this calculation is sketched in Fig. 4. The angular radius of both the Sun and Moon as viewed by MODIS are small enough ($\sim 0.25°$) that they can be treated as overlapping two-dimensional disks, where the radii are defined as the angular radii viewed by MODIS. The angular radius of the Sun and Moon, $R_S(t)$ and $R_M(t)$ respectively, depend on time because of the continuous change in the spacecraft-Sun and spacecraft-Moon distances (see Fig. 4). The distances are derived for each scan using SPICE and combined with the known values of 6.957×10^8 m for solar radius, 1.7374×10^6 m for lunar radius.

The ratio of eclipsed total solar radiance to regular total solar radiance is calculated by taking the ratio of the $\Gamma(r,\lambda)$ integral over the eclipse geometry to the integral over the full solar disk, which is given by

$$A_{eclipse}(\lambda,t) = \frac{\int_0^{R_S(t)} \int_{\theta(r,t)}^{2\pi-\theta(r,t)} \Gamma(r,\lambda,t) r \, d\theta dr}{2\pi \int_0^{R_S(t)} \Gamma(r,\lambda,t) r \, dr}, \tag{6}$$

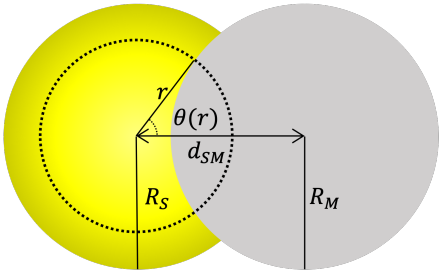

Figure 4: Schematic of the integration over the eclipsed solar radiance for the solar limb darkening model. Note that R_S, R_M, and d_{SM} are time-dependent and calculated each scan.

where $\theta(r,t)$ defines the range of the angular integration so that at each time (i.e. scan), it is determined by the relative position of the Sun and the Moon. The solar intensity function, $\Gamma(r,\lambda,t)$, is time-dependent only through the calculation of $R_S(t)$ every scan. The value of $\theta(r)$ can be calculated from simple geometric arguments involving R_S, R_M, and d_{SM}, the angular distance between the center of the Sun and Moon disks.

We now have two calculations for the Sun fraction, $A_{eclipse}$: "Measured" as the ratio of recorded MODIS SD dn^*, and "Modeled" as the partial solar disk radiance integration that depends on the timing and geometry of Terra MODIS SD calibration events. These are calculated for each band, detector, and mirror-side for each of the eclipse events in Table 1. For clarity, the solar radiance reduction stated in the table is simply the complement of the Sun fraction, such that: solar reduction = 1 - Sun fraction.

4. RESULTS

In this section, we present a description of our results and analysis for the 7 partial eclipse events from Table 1. These represent radiance reduction for the MODIS RSB SD measurements ranging between 3% and 89%, with variations depending on band and detector response.

4.1 Comparing measurement and model trends

Our first presentation of results is shown in Fig. 5 as a comparison between the modeled and measured Sun fraction for 6 of the events listed in Table 1. The measure of the Sun fraction at the center of the sweet-spot range for the SD calibration measurement is plotted as a function of band wavelength for bands $1-19$ and 26. Each symbol corresponds to one detector and mirror-side, so the point spreads represent the relative deviation for detectors within a band. The mirror-side values are too close to be distinguished in the presented scale. The different symbol colors correspond to the different band groupings according to their sensitivity and resolution, with the "Ocean" bands ($8-16$, blue symbols) showing the smallest spread. The modeled Sun fraction with a 1% variance spread is shown as a shaded gray area. Dark gray symbols represent the measured responses for the SWIR bands $5-7$, which are not included in our analysis because of known issues with significant thermal leak and electronic crosstalk contamination.[1] We note that the SWIR points have a relatively small scatter and are within or close to the model prediction spread (shaded area) for the larger Sun fractions (representing a smaller reduction in radiance), as best shown in the two top panels of Fig. 5. However, these measured points go off the chart for the smaller Sun fractions, as expected due to the increased effect of crosstalk contamination at lower signals for each of the detectors in the SWIR bands $5-7$.

The modeled Sun fraction includes the limb darkening component, which controls the wavelength dependence. We can see that in the model line in the different panels of Fig. 5. The variation in curve shape, from more convex to more concave, between the events is related to the fraction of the Sun that is eclipsed in the calculation, based on the event's geometry. When the Moon covers the center of the Sun during the event, the limb consists of a larger fraction of visible light, and wavelengths towards the bluer range become more attenuated, as seen in the 2014, 2015, and 2018 events. When the Moon covers part of the Sun's limb and not the center, the longer wavelengths become more attenuated, as demonstrated by the 2007, 2012, and 2019 events.

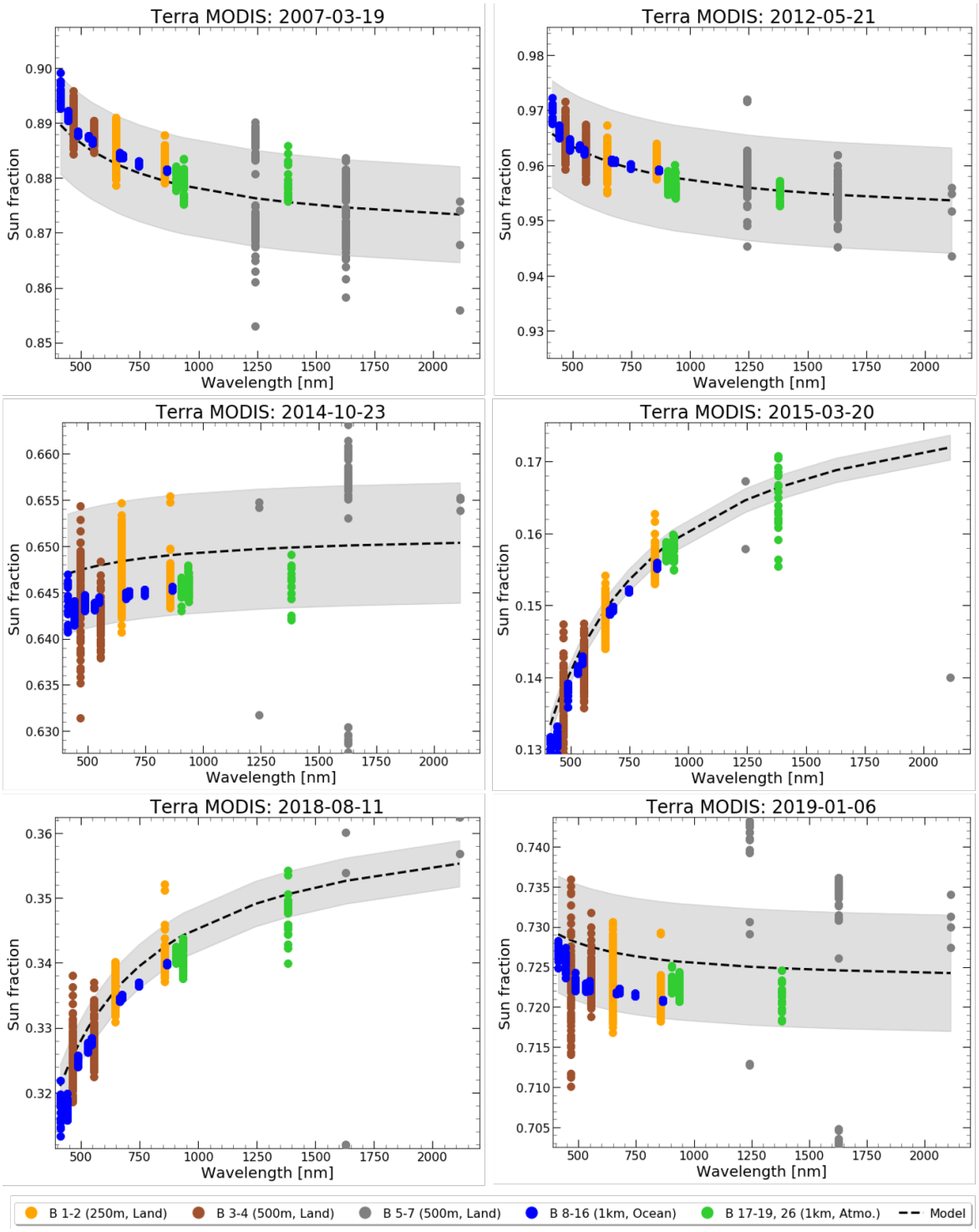

Figure 5: Sun fraction as function of band wavelength for 6 partial eclipse events, with a comparison of measured SD signal reduction (color symbols) to the modeled radiance reduction (black dashed line). The different RSB bands are noted in different colors, divided by their respective resolution (see legend, including a notional designation of their main measurement targets – Land, Ocean, Atmosphere). All results are shown for the SD sweet-spot center (elevation of 12.5 deg) and the multiple points for each band (wavelength) represent the spread in detectors and mirror-sides. Dark gray points represent SWIR bands $5-7$, which are not taken into account in this study. The light-gray contour represents the 1% spread around model prediction.

We can see from Fig. 5 that the general trend across all bands follows the model prediction line. For partial eclipse events that have solar radiance reduction $<\sim 35\%$ (2007, 2011, 2012, 2014 and 2019 events), we can see that the data generally fall within the 1% spread around the model prediction line for most detectors and mirror-sides. For the deeper eclipse events (2015 and 2018 events), there is a more significant deviation, although the median response over all bands and detectors still follows the trend within the variance spread. This indicates that the model is reasonably accurate and that the detector response is not deviating significantly from linearity, as long as the raw signal is not too low. From the result analysis of this study we can qualify this last statement as measured radiance reduction equivalent to $\sim 65\%$ and higher. This is a higher threshold than the one shown from a similar analysis of the VIIRS RSB response on-board the S-NPP and N20 satellites.[2] This may be due to a general "drift" from linearity, with longer mission lifetime and more progressed degradation of the SD mechanism.

We note that the detector response spread we measure could have some component attributed to random instrument noise. Since Terra MODIS has only SD screen closed observations, the SD radiance signal-to-noise ratio can be lower than typical values. For non-eclipsed calibration measurements, the signal-to-noise of Terra MODIS RSB is several 100s for bands $1-8$, $17-19$, and 26, and between $1000-1500$ for bands $8-16$ at the SD radiance level.[1] The signal is averaged over 50 frames per scan at the 1 km resolution bands $(8-16,\ 26)$ and several SD scans per orbit. The variation in the calibration factor ($m1$) is kept under 0.2% in most cases, so detector spreads larger than this value, as shown in Fig. 5, are more likely to be significantly affected by a systematic response to the reduced radiance during and eclipsed calibration event.

4.2 Identifying outlier behavior

We now turn to the potential utilization of partial eclipse events in the data set as tools to identify nominal and outlier behavior. This is related to the assumption of gain linearity mentioned in Sec. 1 as a function of band, detector, and mirror-side, at varying radiance levels.

Fig. 6, 7, and 8 show the ratio of measured to modeled eclipse response for bands 2, 10, and 26, respectively. These are the only bands that showed pronounced features related to the trend of decreasing solar radiance. All events are shown, ordered by increasing radiance reduction, such that the top left panel (2012 event) and bottom right panel (2015 event) correspond to the shallowest and deepest eclipse events, respectively. In each panel, we plot the ratio at the center of the sweet-spot at elevation angle of 12.5 degrees as a function of detector position for both mirror-sides. The y-axis scale is kept identical in all panels and figures.

In Fig. 6, we can identify a feature related to two specific detectors 29 and 30 in band 2. All detectors show a similar behavior as the radiance level decreases (from top left to bottom right panels), within a small variance around the mean value of the ratio across detectors that shifts from above to below the unity line between the panels. However, starting at a radiance level of 27% (2019 event), it is clear that detectors 29 and 30 start to deviate and show increasing out-of-family behavior relative to the rest of the detectors for both mirror-sides. This location is noted in Fig. 6 by the two black dashed horizontal lines. At the highest radiance reduction level (2015 event), these two detectors show the strongest deviation, well above the noise level that the other detectors exhibit. The increase in deviation is correlated with the decrease in radiance level and is an indication that detectors 29 and 30 in band 2 experience low-signal contamination.

It is worth noting that this behavior has been identified and characterized independently as electronic crosstalk contamination of these specific detectors. It was identified in Earth view images of Terra MODIS band 2 as two sets of anomalous pixels. An analysis of lunar images and Spectroradiomatric Calibration Assembly (SRCA) observations concluded that the main contamination contribution is from band 16 detector 10.[8] Further analysis of the electronic crosstalk for band 2 indicated that the contamination may occur before the analog-to-digital signal conversion, but it was unable to be determine for Terra MODIS because the contamination at high sending signal levels may be associated with saturation of the sending band (band 16).[8] Our analysis does not include the specific crosstalk correction that is applied to Terra MODIS RSB calibration operations, and thus shows that at low radiance levels, which correspond to $66\% - 84\%$ reduction for the 2018 and 2015 events, the anomalous behavior of detectors 29 and 30 becomes more pronounced. For the Terra MODIS status of calibrations with a closed SD screen, which is relevant for all eclipse events,,[1] none of the bands are saturated. Thus, at these

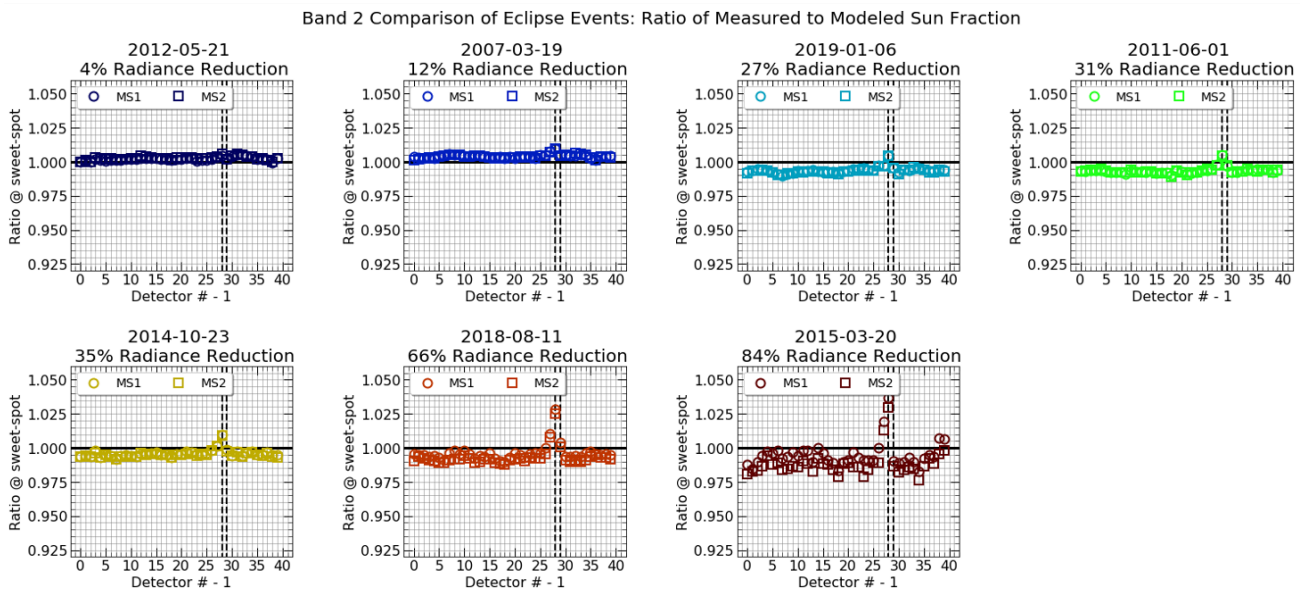

Figure 6: Band 2 comparison of all events, side-by-side, where order of panels is by increasing eclipse depth (i.e. radiance reduction). Each panel shows the ratio of measured to modeled signal at the sweet-spot center per mirror-side (sub-frame 1) as a function of detector position. Note that the detector number on the x-axis is shifted by 1. We note that 2 detectors, 29 and 30, have increasing differences from the trend of other detectors with decreasing radiance level.

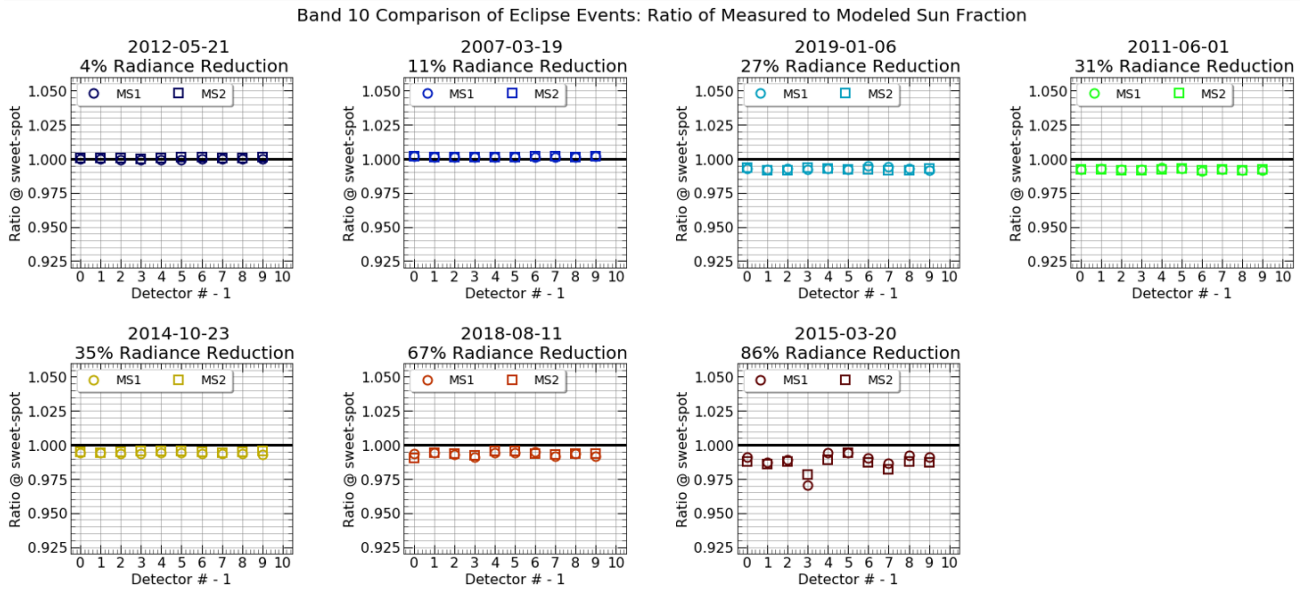

Figure 7: Band 10 comparison of all events, side-by-side, where order of panels is by increasing eclipse depth (i.e. radiance reduction). All plots are formatted identically to those in Fig. 6. We note a potential minor outlier behavior for detector 4, but only at very low radiance (corresponding to low signal-to-noise ratio).

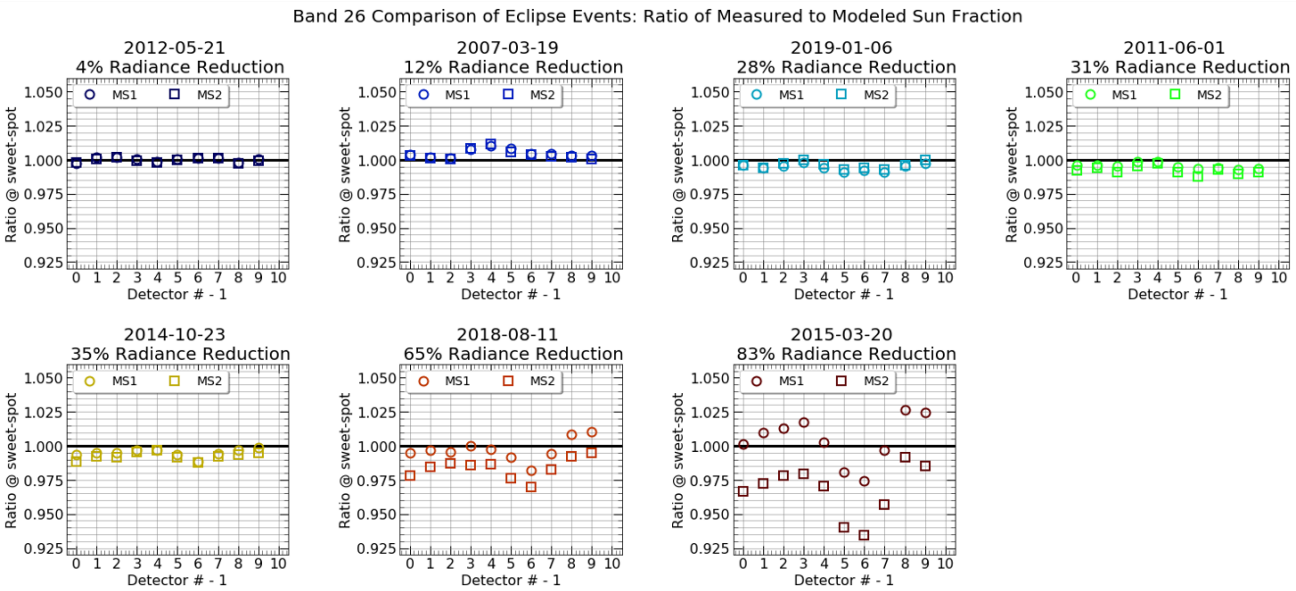

Figure 8: Band 26 comparison of all events, side-by-side, where order of panels is by increasing eclipse depth (i.e. radiance reduction). All plots are formatted identically to those in Fig. 6. We note an undulation trend across all radiance levels, but most notably at a reduction level $> 30\%$. This could be an indication of low-level contamination spread out over a large detector area.

radiance levels, there is no impact of saturation. Hence, our analysis provides independent, yet somewhat indirect, strength to the conclusion of similar crosstalk contamination for Aqua and Terra MODIS.

Fig. 7 shows a feature that resembles in behavior to the band 2 analysis shown in Fig. 6. Here, band 10 detector 4 shows a small out-of-family deviation, but only at a very low radiance level (86% of solar radiance). This corresponds to low signal-to-noise ratio and a contamination level that may be $\sim 50\%$ of that identified for band 2. Since Earth view images are usually above this radiance level, and the SD calibration signal-to-noise level is higher than this for band 10, it is likely only a minor feature. However, this could be an indication of an initial occurrence of crosstalk contamination or deviation from gain linearity unrelated to crosstalk issues, which can intensify in the future and thus may warrant specific monitoring. Further study is needed to determine the source for this feature.

A somewhat different behavior is shown in Fig. 8, where there are no specific outlier detectors, but rather a trend emerges over all detectors. At radiance reduction levels greater than 30%, we can see an undulation trend, which preserves its shape across the detectors, but grows in amplitude and appears to become distinct for each mirror-side. We note here that in our analysis, we did not apply the short-wave IR crosstalk correction that is used in routine Terra RSB calibration activities for bands 5-7 and 26 and for which extensive analysis has been carried out to characterize and minimize its effect.[1] This may be an indication of low-level contamination spread across the array, similar to that which has been identified and characterized for several Aqua MODIS mid-wave IR bands.[9] During lunar observations, it was found in Aqua MODIS bands 20 and 22-25 that an extended region of faint contamination signal was present next to the main lunar image, and it affected all the detectors of the receiving bands.[9] However, no such analysis was conducted for any of the Terra MODIS bands. Despite this, we conclude that the deviation behavior we observe is more likely related to the short-wave IR crosstalk effects mentioned earlier.

As shown in Fig. 8, there is another feature that ramps up as radiance level decreases; namely, a separation between the mirror-sides, where the detector trend remains, but the mirror-side specific response deviates in overall amplitude (see Fig. 8, bottom right panel, for the 2015 event). This feature shows up for other bands as well, except for the high-gain bands 8-16. In Fig. 9, we plot the detector-averaged mirror-side ratio as a

function of the radiance reduction level for each MODIS RSB, but excluding the SWIR bands 5-7. All bands show at least a small increase in mirror-side response difference as solar radiance decreases, which becomes more pronounced beyond $\sim 30\% - 65\%$ radiance reduction. However, except for bands 3, 4, 8, and 26, all bands show a mean mirror-side ratio value$\leq$ 1%, with the high-gain bands having a mean ratio $\leq$ 0.5%. Bands 3 and 8 are on the short end of the MODIS RSB range, with central wavelengths of 466 nm and 412 nm, respectively, while bands 4 and 26 have central wavelengths of 554 nm and 1382 nm, respectively. Previous analyses showed that the mirror-sides for Terra MODIS exhibit larger discrepancy in the blue wavelength bands up to a few percent.[10] However, this is due to a difference in polarization sensitivity between the two mirror-sides, which will only have a contributing effect if there is a polarization difference between eclipsed and non-eclipsed SD observations. While this may provide some explanation for bands 3 and 8, which would exhibit a stronger mirror-side ratio deviation with reduced signal, it does not fit as an explanation for bands 4 and 26. If we take into consideration that the modeled radiance level has a wavelength dependency, which attenuates either the shorter or longer wavelengths under certain geometric conditions (see Sec. 4.1 and Fig. 5), we can conclude that the mirror-side ratio response for bands 3, 4, and 8 may be controlled by a combination of instrument effects (mirror-side dependent) and solar limb darkening model accuracy. As for band 26, we believe that this behavior is largely due to the fact that we did not apply any type of correction for crosstalk contamination

Since the effects mentioned in this section can have small signal contributions, the low-signal-to-noise circumstances of partial eclipse events are advantageous for identification and characterization analysis.

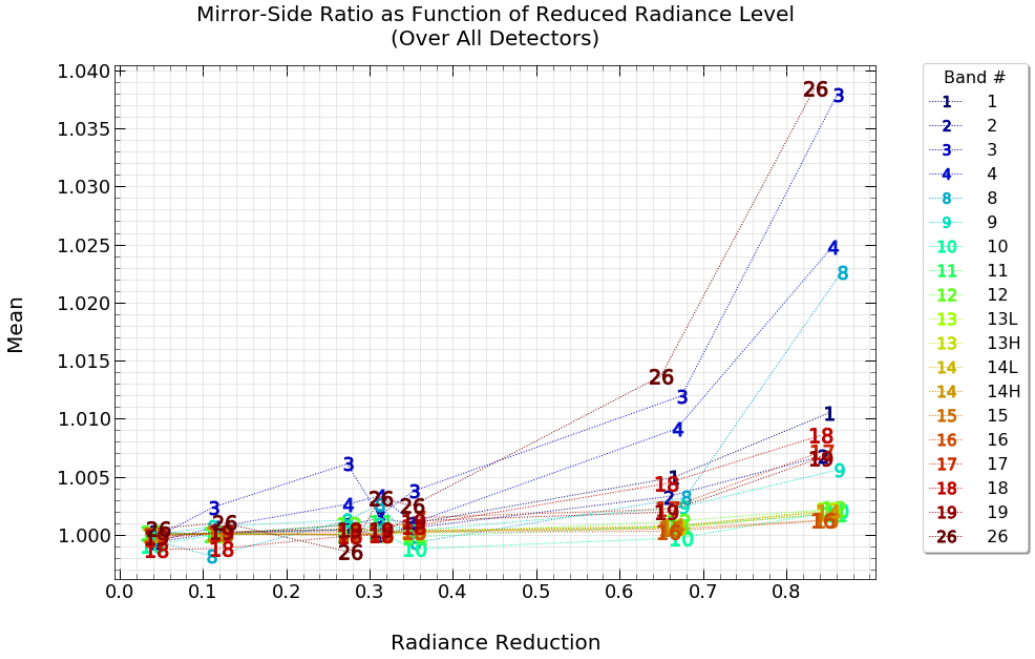

Figure 9: mirror-side ratio (MS1/MS2) of the measured signal during eclipse events as a function of the solar radiance reduction level. We show the mean values for each band averaged over all detectors which are annotated by band name and also color coded. We note that most bands have a mirror-side response difference smaller than 1% for all radiance levels, except for bands 3, 4, 8, and 26, which have a higher mean discrepancy above $\sim$ 60% radiance reduction.

4.3 Comparing with VIIRS data sets

Our study here follows Twedt et al. 2019,[2] where they presented an analysis of partial solar eclipse events observed with the MODIS counterpart instrument on-board the S-NPP and NOAA-20 (N20) satellites. The Visible Infrared Imaging Radiometer Suite (VIIRS) instruments were launched in 2011 (S-NPP) and 2017 (N20) and have been operating in a similar manner to the MODIS instrument in the RSB wavelength range. VIIRS has

RSB bands covering wavelengths from 412 nm to 2250 nm, including moderate-resolution bands (11 M-bands, 16 detectors each) and imaging bands (3 I-bands, 32 detectors each). VIIRS radiometric calibration is maintained similarly to MODIS, with SD calibrations completed every orbit through a fixed attenuation screen, and an SDSM setup to track on-orbit degradation of the SD surface. The identification and processing of the measured data and the model wavelength response at reduced solar radiance were done similarly to the description in Sec. 2 and 3. In their study, Twedt et al. 2019 identified 7 partial solar eclipse events in the existing data set, 5 from S-NPP and 3 from N20. In this sub-section, we compare some of the MODIS results with the VIIRS results and discuss what the combined data set and its trends can tell us about the performance of Terra MODIS.

Although the MODIS and VIIRS RSB bands do not overlap exactly within the MODIS RSB range of $\sim 400 - 1400$ nm, the VIIRS RSB bands M1-7, M9, and I1-2 are closely within the bandwidth of the MODIS bands 1-16 and 26. This wavelength distribution is shown in Fig. 10, 11, and 12, where the bands are annotated by their designation and represented by blue or orange symbols for MODIS and VIIRS, respectively. In these figures, we plot the median of all the measured-to-modeled ratios per band as the central symbol and represent the spreads of the individual detectors and mirror-sides as error bars around the median values. Fig. 10 and 12 differ by the level of solar radiance reduction, where we coupled eclipse events in the MODIS and VIIRS data sets that have a similar range of reduction.

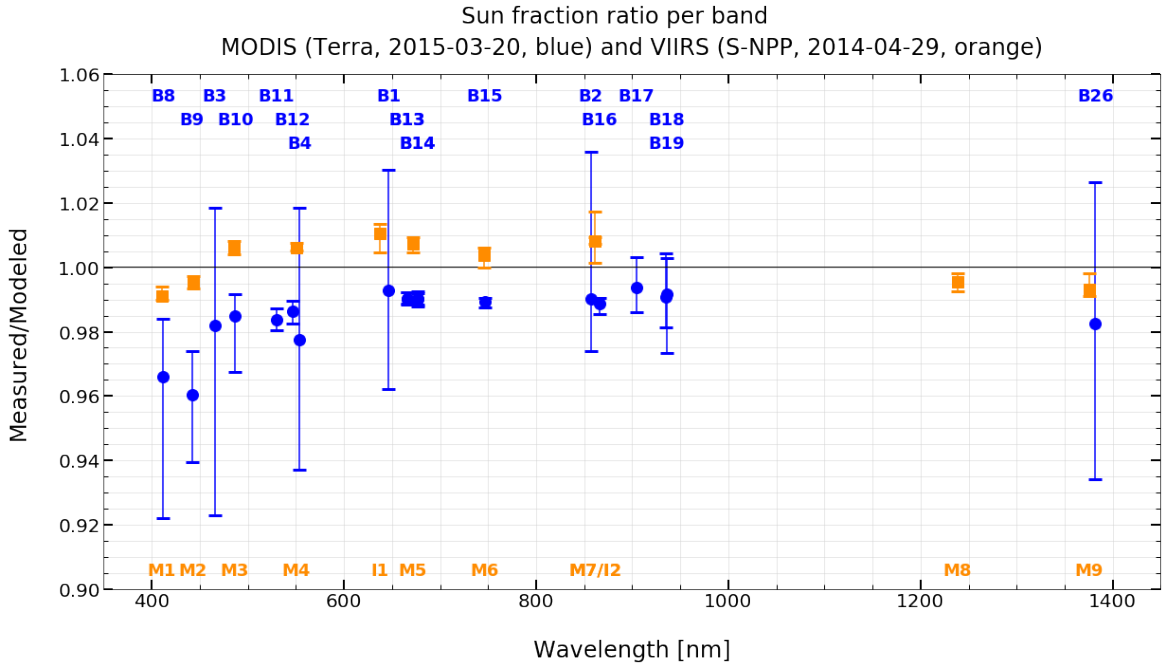

Figure 10: Comparison between MODIS and VIIRS[2] data sets for eclipse events with $\geq 80\%$ radiance reduction. Each point represents the median of the measured-to-modeled reduction factor ($A_{eclipse}$) taken over all detectors for each corresponding RSB band. Error bars represent the maximum and minimum values for each band (see also Fig. 5). MODIS results are in blue, with corresponding notation of RSB band names, and VIIRS results are in orange. We note the similar trend between MODIS and VIIRS data over the comparable bands with similar central wavelengths, especially for the visible-wavelength range. All results have a few percent discrepancy from the model. The MODIS data underestimates the model, while the VIIRS data is within 1% of the model with a small overestimate of the model for the visible bands.

Fig. 10 shows the 2015 MODIS event ($83\% - 89\%$) compared with the 2014 S-NPP VIIRS event ($76\% - 84\%$). These are the deepest eclipse events in any data set we have, and we therefore expect to find larger deviations from the model and potentially more indication of gain non-linearity or signal contamination. We can clearly see that the VIIRS data have significantly less scatter around each band median and are within 1% deviation from the model. This deviation from the model could indicate that there are some accuracy issues with the limb

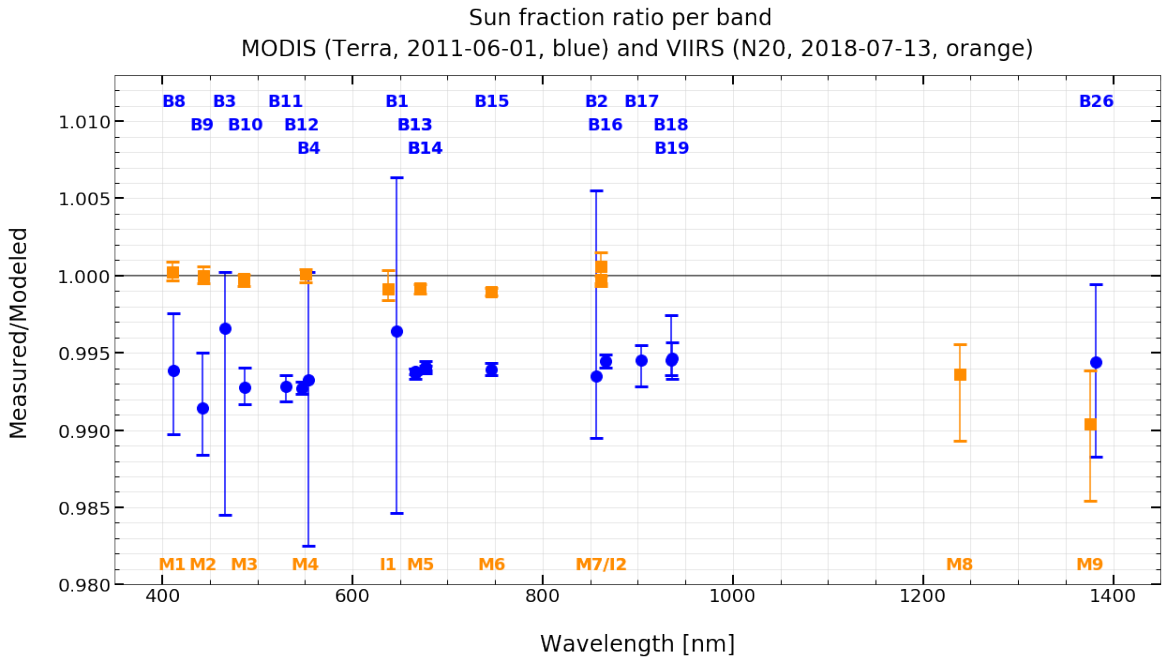

Figure 11: Comparison between MODIS and VIIRS[2] data sets for eclipse events with $\sim$ 30% radiance reduction. Similar to Fig. 10, but with a different y-axis scale. We note that the MODIS and VIIRS trends are still similar for comparable bands, especially in the visible-wavelength. All results are within $\sim$ 1% of the model. MODIS results underestimate the model, while VIIRS results fit the model within 0.2% for the vis bands.

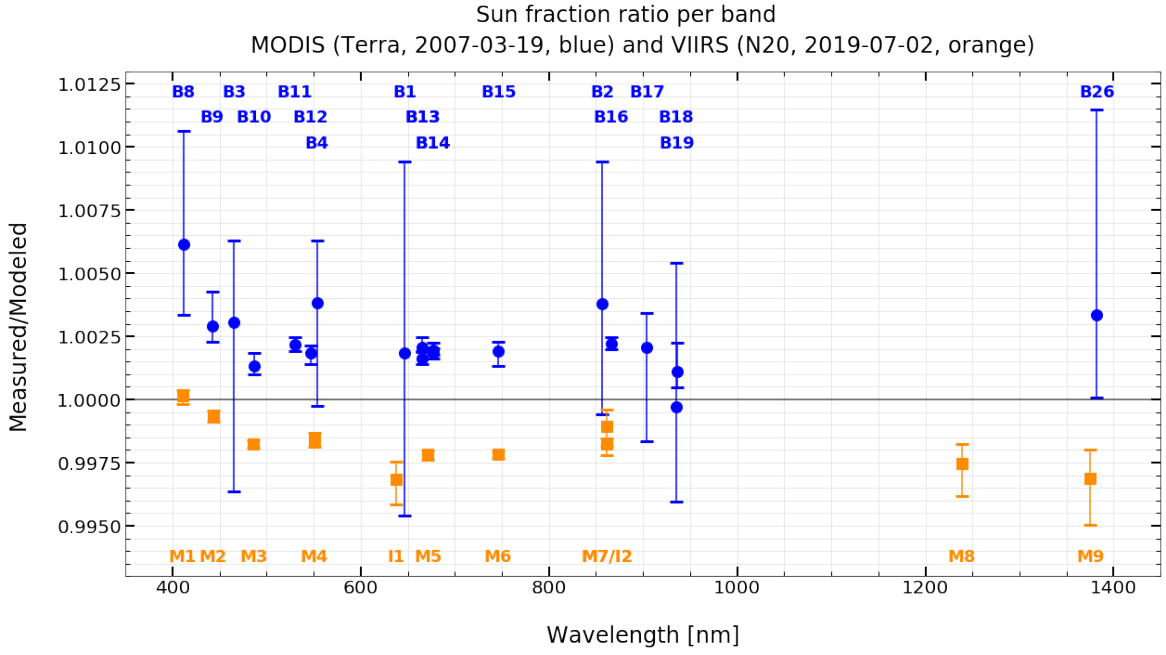

Figure 12: Comparison between MODIS and VIIRS[2] data sets for eclipse events with $\sim$ 10% radiance reduction. Similar to Fig. 10, but with a different y-axis scale. We note that the MODIS and VIIRS trends are still similar for comparable bands, especially in the visible-wavelength. All results are within $\sim$ 1% of the model. MODIS results overestimate the model, while VIIRS results underestimate the model.

darkening model or that there are systematic problems with the gain characterization. Previous analysis of the VIIRS data set concluded that this is a contributing factor indicating good performance stability. The MODIS data, while including more scatter and clearly underestimating the model prediction, is still following the same wavelength trend as the VIIRS data.

Fig. 11 shows the 2011 MODIS event ($30\% - 32\%$) compared with the 2018 N20 VIIRS event ($30\% - 35\%$). We see that the trends over wavelength are still similar here, and both MODIS and VIIRS results are within $\sim 1\%$ of the model prediction. The visible bands fit of the VIIRS data and the model are within $\sim 0.1\%$, which is very similar to the calibration factor (F-factor) orbit-to-orbit variation.[2] Fig. 12 shows the 2007 MODIS event ($10\% - 12\%$) compared with the 2019 N20 VIIRS event ($8\% - 13\%$). We note here that the similarity in trends between the MODIS and VIIRS data still remains, especially up to ~ 900 nm. All results are again within 1% of the model prediction, but this time the VIIRS data underestimates the model prediction, while the MODIS data generally overestimates the model.

In general, as a function of the radiance reduction level, it seems that the MODIS data shift from overestimation to underestimation of the solar limb darkening model as radiance decreases. The VIIRS data shift in an opposite trend, from slight underestimation to slight overestimation of the model as the radiance reduction level decreases. Both data sets seem to have a similar crossing point around a radiance reduction level of $\sim 30\% - 35\%$, where the deviations of the measured response from the model is minimal. This holds true mostly for the visible wavelength range of $400 - 1000$ nm.

While we currently do not have a full explanation for this combined behavior, we consider this as an indication of nominal stable performance for Terra MODIS when compared with established stable performance and linear gain response of either S-NPP or N20 VIIRS. If we consider that the low signal-to-noise introduces contamination into the individual signal responses, as shown in Sec. 4.1 and 4.2, then these results indicate that MODIS is trending similarly to VIIRS, but requires a radiance-level-dependent gain calibration to strictly conform with the operative assumption of gain linearity.

5. SUMMARY

We have shown here our results from an analysis of multiple partial eclipse events observed with the Terra MODIS solar diffuser. Each of our results corresponds to an estimate of the gain response compared with a wavelength-dependent model of the solar radiance reduction impacting the MODIS SD surface. In some cases, we can identify and derive an indicator of outlier behavior, which can be band, detector, or mirror-side dependent.

We have shown that eclipse depths ranging between 3% and 89%, with minor variations depending on wavelength (MODIS band), produce a response that depends on the performance of each band and provides a useful validation of the gain linearity of the detectors. As a general conclusion from our analysis, we can say that for most RSBs there is no significant correlation between detector-dependent trend and the SD-observed radiance level. The dependence of signal reduction on the elevation angle at which the SD records the observations is similar within the sweet-spot angle region, with some minor scatter between detectors.

Overall, the measured responses seem to agree with model estimate, within a few percent, especially for shallower eclipses and visible range wavelengths. We have noted that the discrepancy between modeled and measured solar radiance reduction increases with increasing eclipse depth, but generally it is within $1\% - 2\%$. We therefore suggest that identifying and analyzing future eclipse events for Terra, Aqua, SNPP, or N20 will be an effective means to better characterize and understand low signal-to-noise effects, such as crosstalk contamination. For Terra MODIS, we showed the following specific outlier behaviors:

- Band 2 shows discrepancy in detectors 29 and 30, which is correlated with radiance level. Electronic crosstalk contamination of these detectors was identified in previous studies using other analysis methods.[8]
- Band 26 shows undulation behavior across all detectors, which is correlated with radiance level. This is likely due to known issues with out-of-band optical leak and electronic crosstalk.
- Mirror-side dependent response shows differences generally smaller than 1%, but with a weak dependency on the level of reduced solar radiance. There is a change in the trend around $30\% - 50\%$ radiance reduction for the different bands.

- Bands 3, 4, 8, and 26 show a larger mirror-side response difference, with a mean discrepancy of a few percent above a level of $0\% - 60\%$ in radiance reduction.

When we compare the Terra MODIS data set with other data sets, like the N20 and S-NPP VIIRS data sets, we can see an indication of radiance-level dependent calibration to fully characterize the gain linearity over a large range of signal-to-noise ratios. While the overall band-dependent trend between MODIS and VIIRS is similar, there are shifts in the signal response normalized by the model prediction that require further study. We emphasize again here the possibility that this could either indicate there are some accuracy issues with the limb darkening model or that there are systematic problems with the gain characterization. However, with current data, this cannot be considered as a rigorous comparison of the calibration performance between MODIS and VIIRS.

The most significant question relevant to MODIS application in the context of this paper is: Does this study uncover any significant concerns about MODIS calibration quality? The general answer to that is no. Overall, none of the MODIS RSB exhibit major anomalies or deviations from linearity over the range of radiance values that the eclipse events are able to probe. Some detectors show expected deviations due to previously known electronic crosstalk issues and there are also some minor detector and mirror-side differences, which are observed for a few of the bands, but are not yet fully understood.

In general, we can say that studies of the MODIS and VIIRS RSB data sets, which are presented here and in Twedt et al. 2019,[2] show that we can use radiance-level dependent calibrations to characterize the gain linearity. This on-orbit method takes advantage of the stability and accuracy of the solar radiance source. It can prove useful for application with future sensors that also use solar diffusers and will have much more stringent calibration requirements. Such opportunities include NOAA'a JPSS-2 and JPSS-3 satellites, NASA-led missions like CLARREO[11,12] or PACE,[13,14] and the German DLR-managed EnMAP mission.[15] Thus, we encourage dedicated data collection during future predicted solar eclipse events.

ACKNOWLEDGMENTS

We thank other members of NASA MCST for their support, especially Truman Wilson for help with the SPICE toolkit, Amit Angal for help with reviewing analysis results, and Sarah Henderson for help with reviewing the manuscript draft.

REFERENCES

[1] Xiong, X., Aldoretta, E., Angal, A., Chang, T., Geng, X., Link, D., Salomonson, V., Twedt, K., and Wu, A., "Terra MODIS: 20 years of on-orbit calibration and performance," *Journal of Applied Remote Sensing* **14**, 037501 (July 2020).

[2] Twedt, K. A., Lei, N., and Xiong, X., "Using solar eclipse events to validate VIIRS reflective solar band calibration at multiple radiance levels," in [*Sensors, Systems, and Next-Generation Satellites XXIII*], *Society of Photo-Optical Instrumentation Engineers (SPIE) Conference Series* **11151**, 111511M (Oct. 2019).

[3] Morfitt, R., Barsi, J., Levy, R., Markham, B., Micijevic, E., Ong, L., Scaramuzza, P., and Vanderwerff, K., "Landsat-8 Operational Land Imager (OLI) Radiometric Performance On-Orbit," *Remote Sensing* **7**, 2208–2237 (Feb. 2015).

[4] Markham, B. L., Barsi, J. A., Morfitt, R., Choate, M., Montanaro, M., Arvidson, T., and Irons, J. R., "Landsat 8: status and on-orbit performance," in [*Sensors, Systems, and Next-Generation Satellites XIX*], Meynart, R., Neeck, S. P., and Shimoda, H., eds., *Society of Photo-Optical Instrumentation Engineers (SPIE) Conference Series* **9639**, 963908 (Oct. 2015).

[5] Hestroffer, D. and Magnan, C., "Wavelength dependency of the Solar limb darkening," *Astronomy Astrophysics* **333**, 338–342 (May 1998).

[6] Acton, C. H., "Ancillary data services of NASA's Navigation and Ancillary Information Facility," *Planetary Space Science* **44**, 65–70 (Jan. 1996).

[7] Acton, C., Bachman, N., Semenov, B., and Wright, E., "Spice Tools Supporting Planetary Remote Sensing," *ISPRS - International Archives of the Photogrammetry, Remote Sensing and Spatial Information Sciences* **41B4**, 357–359 (June 2016).

[8] Wilson, T. and Xiong, X., "Electronic crosstalk characterization and correction for MODIS bands 1 and 2 using lunar observations," in [*Earth Observing Systems XXIV*], *Society of Photo-Optical Instrumentation Engineers (SPIE) Conference Series* **11127**, 111271X (Sept. 2019).

[9] Keller, G. R., Wilson, T., Geng, X., Wu, A., Wang, Z., and Xiong, X., "Aqua MODIS Electronic Crosstalk Survey: Mid-Wave Infrared Bands," *IEEE Transactions on Geoscience and Remote Sensing* **57**, 1684–1697 (Mar. 2019).

[10] Angal, A., Xiong, X., and Wu, A., "Monitoring the On-Orbit Calibration of Terra MODIS Reflective Solar Bands Using Simultaneous Terra MISR Observations," *IEEE Transactions on Geoscience and Remote Sensing* **55**, 1648–1659 (Mar. 2017).

[11] McCorkel, J., Thome, K., Hair, J., McAndrew, B., Jennings, D., Rabin, D., Daw, A., and Lunsford, A., "Instrumentation and first results of the reflected solar demonstration system for the Climate Absolute Radiance and Refractivity Observatory," in [*Earth Observing Systems XVII*], Butler, J. J., Xiong, X., and Gu, X., eds., *Society of Photo-Optical Instrumentation Engineers (SPIE) Conference Series* **8510**, 85100B (Sept. 2012).

[12] Lukashin, C., Wielicki, B. A., Young, D. F., Thome, K., Jin, Z., and Sun, W., "Uncertainty Estimates for Imager Reference Inter-Calibration With CLARREO Reflected Solar Spectrometer," *IEEE Transactions on Geoscience and Remote Sensing* **51**, 1425–1436 (Mar. 2013).

[13] Gorman, E. T., Kubalak, D. A., Patel, D., Dress, A., Mott, D. B., Meister, G., and Werdell, P. J., "The NASA Plankton, Aerosol, Cloud, ocean Ecosystem (PACE) mission: an emerging era of global, hyperspectral Earth system remote sensing," in [*Sensors, Systems, and Next-Generation Satellites XXIII*], *Society of Photo-Optical Instrumentation Engineers (SPIE) Conference Series* **11151**, 111510G (Oct. 2019).

[14] Meister, G., Knuble, J. J., Cook, W. B., Gorman, E. T., and Werdell, P. J., "Calibration plan for the Ocean Color Instrument (OCI) engineering test unit," in [*Sensors, Systems, and Next-Generation Satellites XXIII*], *Society of Photo-Optical Instrumentation Engineers (SPIE) Conference Series* **11151**, 111511W (Oct. 2019).

[15] Baur, S., Wachter, R., Basili, P., Lettner, M., Mücke, M., Sornig, M., and Fischer, S., "Calibration and characterization of the EnMAP hyperspectral imager," in [*Sensors, Systems, and Next-Generation Satellites XXIII*], *Society of Photo-Optical Instrumentation Engineers (SPIE) Conference Series* **11151**, 111511B (Oct. 2019).